A Multilayer Model of the Thermohaline and Wind-Driven Ocean Circulation

RUI XIN HUANG* AND KIRK BRYAN

Geophysical Fluid Dynamics Program, Princeton University, Princeton, NJ 08542

ABSTRACT

A hybrid, multilayer model for the oceanic general circulation is formulated and tested. The model includes a mixed layer at the surface which is specified by Eulerian coordinates, and three moving layers below which are specified by quasi-Lagrangian, isopycnal coordinates.

Initial tests have been carried out with a 22 × 22 horizontal grid mesh covering a subtropical–subpolar basin (6000 × 6000 km^2). The numerical results demonstrate a strong interaction between the wind-driven and the thermally driven circulations, including outcropping of the lower isopycnal layers, a Gulf Stream-like interior boundary current, and convection which produces mode water and abyssal water. The model provides insight into the potential vorticity balance and its relation to both the wind-driven and thermohaline components of the circulation which has not been previously available from Eulerian numerical models or analytical models based on the assumption of an ideal fluid thermocline.

1. Introduction

The study of thermohaline circulation of the oceans is a formidable task due to strong nonlinearity and complicated boundary conditions. Diffusive adjustment at the base of the thermocline may take a thousand years to reach a statistical equilibrium state, yet the high-frequency processes associated with mesoscale eddies and waves greatly limit the time step allowed in a numerical integration of the governing partial differential equations. Although different ways of accelerating the spin-up process have been implemented (cf., Bryan, 1984; Bryan and Lewis, 1979), the computer time required for a model to reach a thermal equilibrium state is still extremely long.

Recently, Rhines et al. (1985) carried out an extensive study of buoyancy-driven circulation with a quasi-geostrophic (QG) model. Their model emphasizes high horizontal resolution rather than vertical resolution and shows some interesting features of the interaction between the wind-driven and simplified buoyancy-driven circulations. However, QG models are based upon the assumption that the vertical stratification is horizontally uniform within the domain of study. Though this assumption makes the numerical integration much easier, it is not really appropriate for the study of ocean currents in a basin of planetary scale, since in that case the horizontal variation of stratification not included in a QG model becomes an essential feature of the circulation.

Traditional primitive equation models have been written in finite-difference form with Cartesian coordinates. Although similar models have been successfully used for atmospheric dynamics, their application to the oceans may be less appropriate. There is evidence that mixing by mesoscale eddies in the ocean takes place predominantly along isopycnals, and diapycnal mixing is rather small. By parameterizing subgrid turbulence with constant and rather large horizontal mixing, level models introduce a fictitious horizontal buoyancy flux, or equivalently, a large diapycnal mixing in areas of sloping isopycnals. Though some alternatives of overcoming the difficulty have been proposed (cf. Redi, 1982; McDougall and Church, 1986), little progress along this direction has been reported.

A natural alternative is a layered model based on isopycnal coordinates. The advantage of layered models is the ability to resolve a sharp front with only a few layers. Since water masses conserve their own identity on much longer time scales than air masses are conserved in the atmosphere, layered models have a potential of simulating ocean processes much more economically than level models. Admittedly, layered models have disadvantages, such as more complex boundary conditions. Because of the conceptual simplicity of layered models, theoreticians favor this type of coordinate in analytic models, while numerical modelers tend to use fixed vertical coordinates. As a result, there is a significant gap developing between traditional numerical and analytical models. We believe that numerical models with just a few layers may be an effective bridge between these two different approaches.

An analytical multilayer model of the wind-driven circulation was first studied by Welander (1966). His

---

* Present affiliation: Woods Hole Oceanographic Institution, Woods Hole, MA 02543.

---

solution took into account the nonlinear interaction between layers and contained a strong western boundary current with return flow in a second unventilated layer. A much stronger nonlinearity associated with outcropping phenomenon was analyzed by Parsons (1969) using a simple reduced-gravity model. Kamenkovich and Reznik (1972) extended Parsons' (1969) approach to the case involving an outcropped second layer with finite depth. Veronis (1973) studied the world ocean circulation by using an analytical model similar to Parsons' model. Recently, the dynamical structure of the generalized Parsons' model has been examined in detail by Huang (1984) and Huang and Flierl (1987). Due to the assumption of no mass exchange between layers, Parsons' model and its generalizations are limited to purely wind-driven circulations.

Luyten et al. (1983; hereafter LPS) studied a multilayer model for the ventilated thermocline. By imposing the density distribution on the upper boundary, the model implicitly includes heating. Their model closely follows the classical theory of the ideal fluid thermocline in which water particles conserve potential density and potential vorticity along trajectories. The model shows the structure of the ventilated zone and shadow zone. Since the model does not include any dissipation, a question remains of how to represent the currents at the western boundary. It is also unclear how much the neglect of any feedback by the western boundary current affects the interior solution given by such an idealized model. While the LPS model specified the density on the bottom of the surface mixed layer as a given upper boundary condition, this density condition is actually the result of a complex interaction between the mixed layer and the geostrophic flow below it. Pedlosky et al. (1984) have partially addressed this problem in an analytic study which includes a simple mixed layer.

Recently, there have been quite a few theoretical studies on thermally forced circulation (e.g., Luyten and Stommel, 1986; Pedlosky, 1986). Using a constant source/sink distribution in a two-layer formulation, these studies demonstrate a very interesting nonlinear interaction between the wind-driven and buoyancy-driven circulations. Like the LPS model, however, these models are also limited in their ability of simulating the oceanic circulation by specifying a priori the diapycnal velocity between layers for the interior ocean and ignoring the western boundary region. Accordingly, a simple multilayer model for a closed basin is called for in order to extend present insight on large-scale circulation.

Rhines and Young (1982) studied the nonlinearity associated with multilayer models from a quite different point of view. According to their theory, strong wind forcing can distort the interface so much that closed potential vorticity isopleths appear in the subsurface layers along which water particles are free to move. Based upon a special form of mixing, a solution is chosen among many possible solutions. Accordingly, these subsurface layers can be divided into inactive regions and pool regions. The pool regions are characterized by homogeneous potential vorticity due to slow cross-streamline mixing as particles make repeated circuits along closed streamlines.

Originally, Rhines and Young's (1982) theory of potential vorticity homogenization was based on the quasi-geostrophic approximation and an assumption of weak lateral turbulent mixing along isopycnals. Holland et al. (1984) carried out a series of numerical experiments with an eight-level, eddy-resolving model. The results showed vast regions of homogenized potential vorticity in the subsurface levels. Even the boundary between the gyres has been flushed out in the potential vorticity map by the strong eddy activity. However, these numerical experiments correspond to much stronger eddy mixing than envisioned in the analytical theory (Haidvogel, personal communication, 1986).

Numerical experiments with primitive equations (Cox and Bryan, 1984; Cox, 1985) also demonstrate the importance of strong mixing by mesoscale eddies, but in addition, they show the great importance of convection in the subarctic gyre for establishing a rather uniform low potential vorticity in the ventilated waters. Results from eddy-resolving models suggest that the thermocline is far from an ideal fluid. Turbulent transport of potential vorticity along isopycnals is of the same order as the other terms.

Density coordinate was first used by Robinson (1965) in a study of the Gulf Stream. Hodnett (1978) used a density coordinate in a study of the thermocline. Bleck and Boudra (1981, 1986) developed a hybrid (quasi-isopycnic) model and showed initial results for a purely wind-driven circulation which were quite different from the QG models. Recent studies of a two-layer model (Huang and Flierl, 1987; Huang, 1986) and a three-layer model (Huang, 1987) confirm the drastic difference between QG models, which ignore the layer thickness change, and layered models which include the strong nonlinearity associated with the layer thickness change. The most important result is that strong wind forcing causes the lower layer to outcrop and a strong interior boundary current thus formed unifies two gyres into a strong circulation system which is highly asymmetric with respect to the zero-wind-curl line. Potential vorticity maps from this kind of model are distinctly different from those produced by the QG models.

Modeling an outcropping line in an isopycnal coordinate system is not simple because outcropping is usually associated with a sharp front. A special algorithm, the flux-corrected-transport (FCT) (see Boris et al., 1973; Zalesak, 1979) algorithm, which combines the advantage of the stable character of a first-order difference scheme and the sharp resolution of a second-order scheme, has been proven to be very useful in this

situation (cf. Bleck and Boudra, 1981, 1986; Bougue et al., 1986).

To explore the classic concept that mixing is predominantly along isopycnals, and to answer some remaining questions raised by previous models, we have been motivated to develop a multilayer (isopycnic) model for the oceanic circulation. Since the wind forcing, thermal forcing, and the vertical turbulent mixing strongly dominate the dynamic processes in the surface layer of the ocean, a purely isopycnal model is not appropriate. To combine the advantage of both the Eulerian and the Lagrangian coordinates, a hybrid model is introduced. Density coordinates are used to represent several moving layers below the mixed layer, while Eulerian coordinates are used to represent a surface mixed layer. Since the layer adjacent to the mixed layer is strongly dominated by the Ekman pumping or suction, it takes at least three moving layers to show the potential vorticity distribution in the subsurface layers and its role in the basin-scale thermohaline circulation. The model is forced by both wind stress and buoyancy flux acting on the upper surface.

The aim of this study is to describe the method and illustrate it with a single reference state in which both wind and buoyancy driving are important. Further study of the physical processes in the model will be provided by comparing the reference solution to asymptotic cases of no wind driving or no buoyancy driving and these will be presented in upcoming papers.

2. The formulation of the model

a. The mathematical model

The model is intended to simulate the steady circulation, including a subtropical and subpolar gyre in a rectangular basin. The ocean is forced from above by both wind stress and buoyancy flux. The vertical stratification may be modeled by an arbitrary number of layers, but we will choose five layers for illustration.

There is a mixed layer on the top which has a constant depth and a horizontally variable density. Below the mixed layer there are four layers. Each of them has a fixed density, but variable depth. The lowest layer is assumed to be infinitely thick and motionless. No heat flux is allowed through the interface between the deep resting layer and the active layers above. The overall structure of the model is shown in Fig. 1. The choice of a deep resting layer as a lower boundary condition is a convenient assumption of the model, but not an essential feature. Alternatively, we could have adopted a more conventional approach with a rigid bottom condition, and the added constraint that the vertically integrated transport is divergenceless in the horizontal plane (Bryan, 1969). The nondivergent constraint effectively filters out high-frequency gravity waves from the model, but at the cost of added complexity. This feature could be added in cases where detailed verification with data is the primary aim.
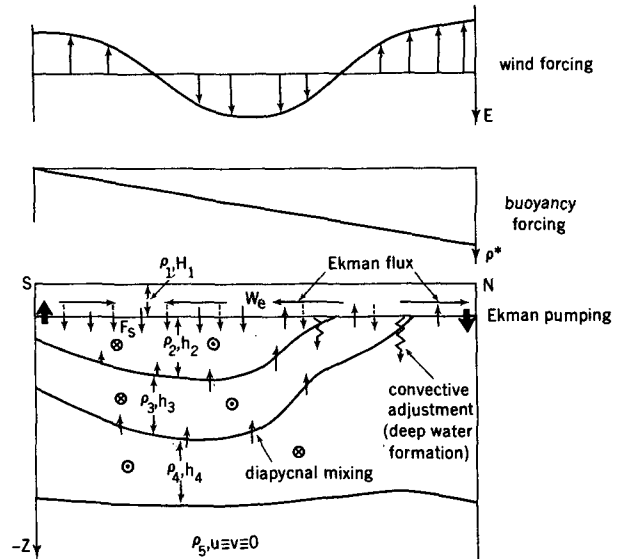

FIG. 1. A schematic diagram of the model. The model is forced from above by a zonal sinusoidal wind and a buoyancy forcing. There are three moving layers below the mixed layer. All layers interact through Ekman pumping, diapycnal mixing, and interface friction. Intermediate and deep water are formed by convective adjustment in the subpolar basin. Heavy arrows indicate strong upwelling (downwelling) along the boundaries.

Starting from the top of the ocean, the velocity and temperature fields at each space gridpoint are calculated by equations in Eulerian form. The mixed layer interacts with layers below through interface friction and vertical mass exchange. The divergence within the mixed layer which drives the vertical mass exchange with the layers below is mainly associated with Ekman transport, but there are other factors associated with the beta effect and friction, as well.

1) MOMENTUM EQUATIONS

Our main interest is modeling the large-scale circulation on a climate time scale. For this case it is easy to prove that both the time-dependent terms and the inertial terms in the horizontal momentum equations are relatively small and can be neglected (cf., Huang, 1986). Therefore, we can write down the momentum equations for our model

$$-fH_1v_1 + k_1(u_1 - u_2)$$
$$= -H_1P_{1x}/\rho_0 + A_m\nabla(H_1\nabla u_1) + \tau/\rho_0 \quad (1)$$

$$fH_1u_1 + k_1(v_1 - v_2) = -H_1P_{1y}/\rho_0 + A_m\nabla(H_1\nabla v_1) \quad (2)$$

$$-fh_iv_i + k_{i-1}(u_i - u_{i-1}) + k_i(u_i - u_{i+1})$$
$$= -h_iP_{ix}/\rho_i + A_m\nabla(h_i\nabla u_i) \quad (3)$$

$$fh_iu_i + k_{i-1}(v_i - v_{i-1}) + k_i(v_i - v_{i+1})$$
$$= -h_iP_{iy}/\rho_i + A_m\nabla(h_i\nabla v_i) \quad (4)$$

$$i = 2, 3, 4 \quad \text{and} \quad u_5 = v_5 = 0$$

where H_1 is the mixed layer depth, h_i, u_i, v_i are the thickness and velocity for the ith layer, k_1, k_i, k_{i-1} are coefficients for the corresponding interface friction, A_m is the lateral momentum mixing coefficient, ρ_0 is the reference density, and ρ_i is the density for the ith layer. Assuming the lowest layer is stagnant, the pressure gradient in each layer can be calculated by integrating the hydrostatic equation upward:

$$\nabla P_{i-1} = \nabla P_i + g(\rho_i - \rho_{i-1})\nabla Z_{i+1/2} \quad (i = 4, 3, 2)$$

where

$$Z_{i+1/2} = \sum_{j=1}^{i} h_j \quad (i = 4, 3, 2) \tag{5}$$

is the interface depth and ρ_i, ρ_{i-1} are the density of the ith and $(i-1)$th layer. The pressure gradient in the mixed layer is calculated at the middle depth of the mixed layer

$$P_{1x}/\rho_0 = \frac{1}{2}\rho_{1x}gH_1/\rho_0 + P_{2x}/\rho_2. \tag{6}$$

Both vertical and horizontal friction are introduced in the model. Zero normal velocity is the lateral boundary condition for the momentum equations. Since a diagnostic form of momentum equation is used, short baroclinic Rossby waves are excluded from the system described by the partial differential equations. Nevertheless, some short waves do appear in numerical experiments because excluding the inertial terms in the momentum equation makes the system energetically unbalanced and the energy leakage is a continuous source of numerical disturbances. The isopycnal momentum mixing provides a damping mechanism for suppressing these short waves. Since we allow layers to have zero thickness, strong fronts can appear along the edge of these "outcropping" lines. Outcropping here means direct contact with the mixed layer.

The vertical friction is an important momentum carrier in our model which transfers horizontal momentum downward. The interface friction is an essential part of the circulation dynamics. It may be considered a crude parameterization of the effect of vertical momentum transfer by baroclinically unstable mesoscale eddies.

2) BUOYANCE CONSERVATION EQUATION FOR THE MIXED LAYER

In Eulerian coordinates, the buoyance conservation law for the mixed layer is

$$\rho_{1t} + (u_1\rho_1)_x + (v_1\rho_1)_y = (F^b - F^t)/H_1 \tag{7}$$

where F^t and F^b (positive for upward) are the density flux across the upper and lower interfaces due to heat transfer and mass exchange. The upper-surface density flux is parameterized by a simple relation

$$F^t = \gamma(\rho_1 - \rho^*), \tag{8}$$

where γ is the air–sea interaction coefficient, and ρ^* is the equivalent density for a reference state. The lower interface density flux is determined by cross-interface mass exchange and turbulent mixing

$$F^b = W_e\rho_{k'} + F_s \tag{9}$$

where $w_e = H_1(u_{1x} + v_{1y})$ is the vertical velocity across the bottom of the mixed layer (Ekman pumping/suction), $\rho_{k'}$ is the density of the layer adjacent to the mixed layer, F_s is the turbulent density flux across the bottom of the mixed layer. The choice of $w_e\rho_{k'}$ to represent the mass exchange and the expression for F_s will be discussed in the Appendix. Since we allow lower layers to outcrop, the mixed layer can be in direct contact with either the second, the third, or even the fourth layer.

3) CONTINUITY EQUATION FOR LAYERS BELOW THE MIXED LAYER

For the layers below the mixed layer we use density coordinates; thus the corresponding continuity equations have to be transferred to the density coordinates. The general form of density conservation with diffusion is

$$\rho_t + u\rho_x + v\rho_y + w\rho_z = \mu\rho_{zz}. \tag{10}$$

In transferring from the physical coordinates to density coordinates, we have the following relations:

$$\rho_{t,z} = -\rho_{z,t}Z_{t,\rho}$$

$$\rho_{x,z} = -\rho_{z,x}Z_{x,\rho}$$

$$\rho_{y,z} = -\rho_{z,y}Z_{y,\rho}$$

$$w = z_{t,\rho} + uz_{x,\rho} + vz_{y,\rho} + \rho^\# z_\rho$$

$$\rho_{zz} = \rho_z(1/z_\rho)_\rho \tag{11}$$

where $F_{u,v}$ means the partial derivative of F with respect to u, while v is fixed, $\rho^\# = d\rho/dt$ is the "vertical velocity" in the density coordinates. Substituting (11) into (10) yields

$$\rho^\# z_\rho = \mu(1/z_\rho)_\rho = w^* \tag{12}$$

where w^* has a dimension of velocity. It is clear that w^* is the so-called diapycnal velocity due to turbulent mixing. Both the diapycnal velocity w^* and the vertical diffusivity μ have been discussed in connection with many previous models. Recent measurements by Moum and Osborn (1986) confirm a vertical diffusivity of about 1 cm^2 s^{-1}. Since insight rather than detailed simulation is our main motivation, it is more convenient to assume that μ is a constant.

Now for each layer, we have a continuity equation

$$h_{it} + (h_iu_i)_x + (h_iv_i)_y + w^{*t} - w^{*b} = 0 \tag{13}$$

where w^{*t} and w^{*b} are diapycnal velocity at the upper and lower surface of this layer. When the layer is di-

rectly exposed to the mixed layer, w^{*t} should be replaced by W_e, the Ekman pumping/suction velocity. For the fourth layer w^{*b} is zero because we assume no heat flux from the bottom layer.

4) CONVECTIVE ADJUSTMENT

The diapycnal velocity w^* previously discussed specifies the vertical mixing under stable stratification only. Since the model includes buoyancy forcing, loss of buoyancy at the upper surface can create unstable stratification. Since convective overturning is a relatively high-frequency process it is done implicitly in the model through convective adjustment at the end of each time step. Thus, poleward advection in the mixed layer and convection combine in a continuous process which turns the light upper-layer water into dense deep water.

In the hybrid model, the mixed layer has a fixed depth, H_1, and a horizontally variable density, ρ_1. All layers below have fixed density and variable thickness. Thus, the convective adjustment will take place according to the following steps.

(i) If $\rho_1 > \rho_2$, the upper part of a water column is gravitationally unstable and overturning takes place. Dense water in the mixed layer will mix with water in the layer below and attain to a stably stratified new state. This mixing process is illustrated in Fig. 2a. The extra dense water in the mixed layer has to mix with water below and attains new density. Since the model only allows for discrete density intervals, the intermediate water must have a density ρ_3 and thus sinks to the third layer. As the result of the mixing, the density in the mixed layer is reduced to ρ_2 and the interface between the second and third layer moves upward, while the fourth layer is undisturbed by this adjustment. By a simple density conservation, we have

$$\Delta h(\rho_3 - \rho_2) = H_1(\rho_1 - \rho_2). \qquad (14)$$

Thus, after the adjustment

$$h_2 = h_2{}^0 - H_1(\rho_1 - \rho_2)/(\rho_3 - \rho_2) \qquad (15a)$$

$$h_3 = h_3{}^0 + H_1(\rho_1 - \rho_2)/(\rho_3 - \rho_2) \qquad (15b)$$

$$\rho_1 = \rho_2. \qquad (15c)$$

Note that both volume and buoyancy are exactly conserved in the adjustment process.

(ii) After the first step of density adjustment, h_2 may become negative. This is the case shown in Fig. 2b. Since each layer should have a nonnegative thickness, there is a second step in the adjustment process. Within this step the density in the mixed layer is increased in such a way that the total density is conserved and the interface between the third and fourth layer is undisturbed, thus

$$\rho_1{}^0 H_1 + \rho_2 h_2{}^0 + \rho_3 h_3{}^0 = \rho_1 H_1 + \rho_3 h_3 \qquad (16)$$

$$h_3 = h_2{}^0 + h_3{}^0. \qquad (17)$$

Therefore, the end state is

$$\rho_1 = \rho_1{}^0 - h_2{}^0(\rho_3 - \rho_2)/H_1 \qquad (18a)$$

$$h_2 = 0 \qquad (18b)$$

$$h_3 = h_2{}^0 + h_3{}^0. \qquad (18c)$$

(iii) If $\rho_1 > \rho_3$ after the second step has been taken, there is a step similar to step (i) which can make the vertical stratification stable. By a similar argument, the end state is

$$\rho_1 = \rho_3 \qquad (19a)$$

$$h_3 = h_3{}^0 - H_1(\rho_1 - \rho_3)/(\rho_4 - \rho_3) \qquad (19b)$$

$$h_4 = h_4{}^0 + H_1(\rho_1 - \rho_3)/(\rho_4 - \rho_3). \qquad (19c)$$

A similar step is needed to adjust the density profile if h_3 is negative in the end of the previous step and this
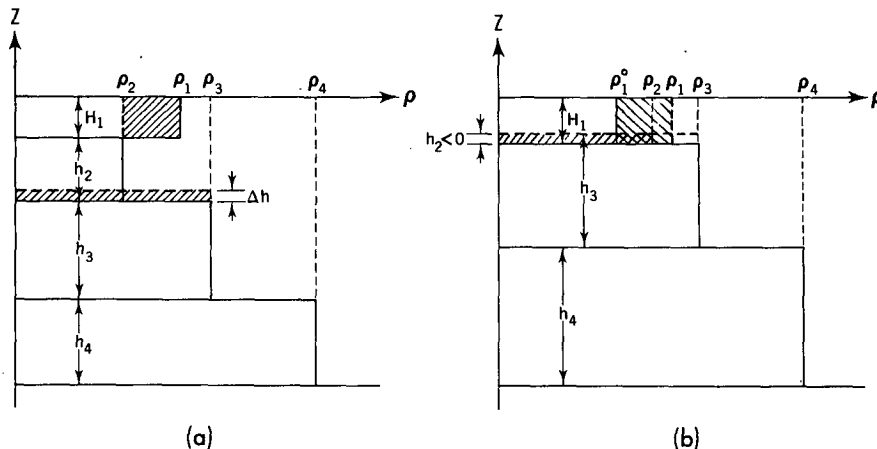

FIG. 2. A schematic diagram for the convective adjustment process.

process continues till the whole water column becomes gravitationally stable.

b. The numerical model

The numerical model used in this study solves a diagnostic form of the momentum Eqs. (1, 2, 3, 4) and the time-dependent form of the buoyancy conservation (7) and the continuity Eq. (13). To facilitate the description of the numerical scheme the following operators are defined:

$$\delta_x f = (f_{i+1/2} - f_{i-1/2})/\Delta x \qquad (20)$$

$$\bar{f}^x = (f_{i+1/2} + f_{i-1/2})/2. \qquad (21)$$

We make use of what Messinger and Arakawa (1976) describe as a "B" grid. If we think of the grid in the horizontal plane as a chess board, the thicknesses are defined at the center of the squares and the horizontal velocities are defined at the corner points. The subsequent equations for the density of the mixed layer and the layer thicknesses can be put in finite difference form.

$$\rho_1{}^{n+1} = \rho_1 + \Delta t \cdot FCT(u_1, v_1, \rho_1) + \Delta t(F^b - F^t)/H_1 \qquad (22)$$

$$h_i{}^{n+1} = h_i + \Delta t \cdot FCT(u_1, v_1, h_1)$$
$$+ \Delta t(W^{*t} - W^{*b}), \quad i = 2, 3, 4. \qquad (23)$$

The superscript n is understood on all variables without superscripts. The vertical mass flux through the base of the mixed layer is

$$W_e = H_1(\delta_x \bar{u}^y - \delta_y \bar{v}^x) \qquad (24)$$

and the diapycnal velocity w^* can be calculated from (12). As shown in Fig. 3, to calculate the diapycnal velocity across the interface at $z = z_2$ we need the density gradient at the middle of the second and third layers. Assuming the density at the bottom of the mixed layer is ρ_1 and the density at the interface between second and third layers is $(\rho_3 + \rho_2)/2$, the average gradient of the upper and lower half of the second layer is

$$-\partial\rho/\partial z|_{\rho_2}{}^- = 2(\rho_2 - \rho_1)/h_2 = 2\Delta\rho_1/h_2 \qquad (25)$$

$$-\partial\rho/\partial z|_{\rho_2}{}^+ = (\rho_3 - \rho_2)/h_2 = \Delta\rho_2/h_2. \qquad (26)$$

Therefore, the average density gradient at the center of the layer is

$$-\partial\rho/\partial z|_{\rho_2} = (2\Delta\rho_1 + \Delta\rho_2)/2h_2. \qquad (27)$$

Similarly, we have

$$-\partial\rho/\partial z|_{\rho_3} = (\Delta\rho_2 + \Delta\rho_3)/2h_3, \qquad (28)$$

and so on. Here we treat the boundary between the mixed layer and layer below slightly differently compared with other interfaces. Since the turbulent mixing coefficient used is vertically constant, our choice is just one possible choice.
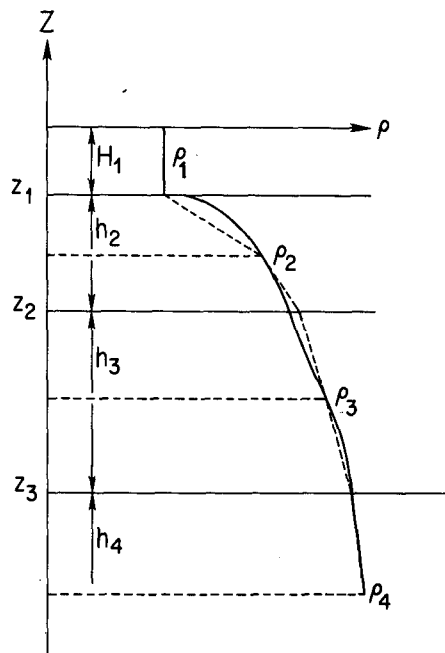

FIG. 3. A schematic diagram of density–depth coordinates. Density is defined at the middepth of each layer. The solid line is the real density profile, the dashed line is the finite difference approximation.

Now the diapycnal velocity crossing the interface between the second and third, and the third and fourth layer is calculated by

$$W_{2,3}^* = -\frac{1}{2}\mu[(\Delta\rho_2 + \Delta\rho_3)/h_3$$
$$- (\Delta\rho_2 + 2\Delta\rho_1)/h_2]/\Delta\rho_2 \qquad (29)$$

$$W_{3,4}^* = -\frac{1}{2}\mu[(\Delta\rho_3 + \Delta\rho_4)/h_4$$
$$- (\Delta\rho_2 + \Delta\rho_3)/h_3]/\Delta\rho_3 \qquad (30)$$

where $\Delta\rho_i = \rho_{i+1} - \rho_i$ is the density jump between the ith and $(i + 1)$th layers, $i = 1, 2, 3$. It is easily understood that w^* is the algebraic sum of two terms based upon the density gradients calculated at the middle of two adjacent layers, and the density gradient calculated at the layer adjacent to the mixed layer has a slightly different form due to the fact that density is vertically homogenized in the mixed layer. When the second layer outcrops, $w_{3,4}^*$ should be calculated by a formula similar to (29).

The turbulent heat flux across the bottom of the mixed layer is, from Appendix Eq. (A5):

$$F_s = \frac{1}{2}\mu[(\Delta\rho_2 + 2\Delta\rho_1)/h_2 - (\Delta\rho_3 + \Delta\rho_4)/h_4]. \qquad (31)$$

Thus, F_s is the sum of two terms. The first term is the turbulent heat flux calculated by using the density gradient at the middle of the layer adjacent to the mixed layer. The second term is a correction calculated by using the density gradient at the middle of the lowest moving layer. For a continuous analogy with the real

oceans with a thermally isolated lower boundary, the density jump for the lowest layers should approach zero and this correction is negligible. Since the present model is highly truncated, the density jump for the lowest layers is nonzero and inclusion of this correction term is an important constraint for global buoyancy conservation of the hybrid model. We have run many numerical experiments to test this heat flux term. Without the second correction term, the model cannot reach a steady state of thermal equilibrium. Only if the correction term is included can the model reach a thermodynamically steady state.

The mass equation is written in a two time-level scheme using the FCT algorithm to maintain a sharp front. The FCT algorithm has been found to be very good at maintaining a sharp front within 2–3 gridpoints without creating any local oscillations between adjacent gridpoints. This is accomplished by computing the layer thickness at each point by combining a first-order donor-cell scheme and a second-order correction in such a way that the prediction is as close to second order as allowed by the constraint that spurious local maxima or minima are excluded. As will be shown in the numerical examples, the present code conserves the mass very well and gives smooth solutions. It should be noticed that there is no numerical smoothing in the thickness prediction other than the numerical diffusion intrinsic to the FCT algorithm.

The x-component of the momentum equation of the second layer is written in the finite-difference form:

$$-f[\alpha(h_2v_2)^{n+1} + (1-\alpha)h_2v_2] + k_1(u_2-u_1)^{n+1}$$
$$+ k_2(u_2-u_3)^{n+1} = -h_2\delta_x\overline{P_2^{n+1}}^y/\rho_0$$
$$+ A_m[\delta_x(h_2\delta_x\overline{u_2}^y) + \delta_y(h_2\delta_y\overline{u_2}^x)]; \quad (32)$$

the u_2 and other velocity components are calculated in a similar way.

The momentum equations are written in a two time-level scheme. The Coriolis terms are treated in a semiimplicit way. From (32) and similar equations for other components of the velocity field, u_i^{n+1}, v_i^{n+1} ($i = 1, 2, 3, 4$) can be solved by inverting an 8×8 matrix.

Our main interest is the final quasi-stationary state of the numerical model. Therefore, the details of the evolution to the final state are unimportant. The time step of the numerical integration is limited by the equialent of Kelvin waves of the model, especially along the southern boundary (cf. Killworth, 1985). To guarantee a smooth spinup, a time step of the order of a day has been chosen based upon a rather conservative estimate.

In the initial tests the basin is a 6000×6000 km² box which is basically a model for the North Atlantic, with the central latitude at 45°N. Thus $f_0 = 1.03 \times 10^{-4}$ s⁻¹ and $\beta = 1.61 \times 10^{-13}$ s⁻¹ cm⁻¹. Accordingly, our model's southern boundary is near 15°N, and the northern boundary near 75°N. The maximum wind forcing is 1.0 dyn cm⁻², the air–sea interaction coef-

ficient is set to $\gamma = 2.5 \times 10^{-3}$ cm s⁻¹ (with a mixed layer depth of 50 m, this is equivalent to a relaxation time of 23 days), and the vertical turbulent mixing coefficient is $\mu = 1.3$ cm s⁻¹. The basin is horizontally covered by a 22×22 mesh (including the boundary points). The model is spun up from a state of rest and has been run for 300 years to make sure that the final equilibrium state has been attained.

3. The numerical results

In this study we have chosen to illustrate the capabilities of the model by describing a single case in which both wind- and buoyancy-driving are important. Other cases in which either wind-driving or buoyancy-driving dominate will be discussed in upcoming papers, which will provide more insight.

A steady state is reached by straightforward integration of the model equations with respect to time. In a problem which includes vertical diffusion, the longest time scale is ordinarily Z^2/μ, where Z is the depth scale and μ is the vertical diffusion coefficient. Since our model represents the thermocline with only a few layers, diffusion in the abyssal water does not come into consideration. The model comes into equilibrium after an integration of 300 years which corresponds to a depth scale of approximately 1 km.

Let us start with the density anomaly pattern in the mixed layer. Since there is only one thermodynamic parameter in the model, the density pattern is directly related to the temperature and heat gain at the sea surface. As one can see from Fig. 4a, there are two regions of cooling, 1) the region of the western boundary current and its outflow region where the warm water from low latitude is cooled down by the air–sea interaction; and 2) the northeast corner where the relatively warm water in the third layer moves northward into the high latitude, is cooled and sinks down to the fourth layer. Both of these two regions roughly correspond to the regions of major heat loss in the North Atlantic in Budyko (1963) heat balance maps. The maximum net heat loss is about 100 W m⁻², which is close to the maximum value of 150 W m⁻² (120 kcal cm⁻²) given by Budyko. The second maximum in the model corresponds to the heat loss near the Norwegian Sea in Budyko's map. A region of strong heat gain is located along the southern boundary of the basin where a solid wall is assumed and a strong upwelling appears to compensate the poleward Ekman flux in the mixed layer. There is a broad region of heat gain in the interior of the basin.

The poleward heat flux is calculated as the sum of the local air–sea heat transfer as defined in Eq. (8). The result is shown in Fig. 4b. The magnitude of the heat flux (maximum of 0.2×10^{15} W s⁻¹) is about half that obtained by Cox (1985). It should be noted that the model's southern boundary is near 15°N, thus the strong upwelling near the equator is not reproduced in the model. The absence of this region may be the major
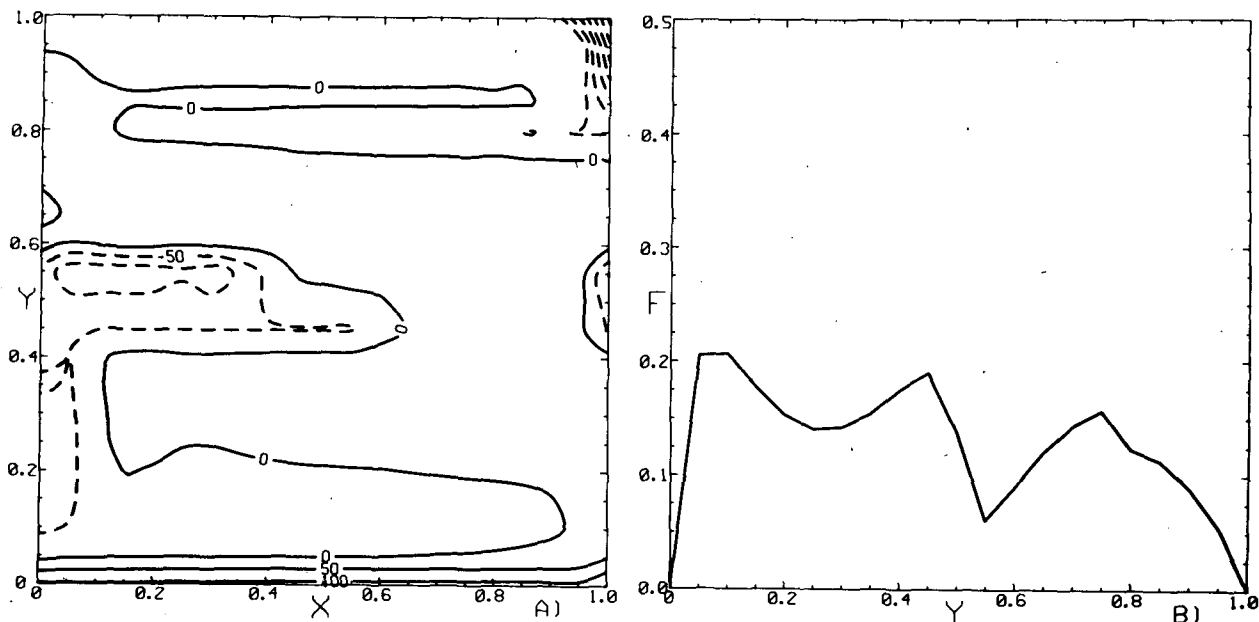
FIG. 4. (a) Net heat gain at the sea surface. Dashed lines for heat loss from the ocean, in units of W m^{-2}.
(b) Poleward heat flux, in units of 10^{15} W s^{-1}.

reason for a greatly reduced poleward heat flux in the model. Furthermore, the model has only three moving layers below the mixed layer. With the same vertical overturning velocity, a model with only a few layers may underestimate the poleward heat flux. In addition, the heat flux curve shows some small irregularities which, presumably, could be smoothed out if there were more moving layers in the model.

The model has included thermal forcing; thus, the upper layers have a continuous mass exchange with lower layers. Figure 5 shows the layer thickness maps which correspond to a hypercritical state discussed by Huang (1987) in which the third and fourth layer outcrop. The second layer ($\sigma = 26.25$) is basically confined to the subtropical gyre. The outcropping line between the second and third layers has a west–east orientation within the western basin. This line, however, turns southeastward in the eastern basin. This south–north excursion of the outcropping line has been reported in a purely wind-driven circulation model (Huang, 1987). This feature is consistent with observations of the North Atlantic (cf. Figs. 6 and 7, McDowell et al., 1982). Apparently, water in the second layer tends to move northward near the eastern boundary. For a wind-driven, multilayer model, this northward movement emerges as an isolated eastern boundary current in the second layer, flowing northward and making up an entire closed loop of boundary currents. In the present model the cooling effect transforms all this water mass flux of the second layer into the third layer as soon as it reaches high latitudes. This convective adjustment process will become clearer in the following discussion.

The thickness map of the third layer, $\sigma_3 = 27.15$, is

shown in Fig. 5b. A front between the third and fourth layers appears in the subpolar basin. The most conspicuous feature is a thickness maximum near the zero-wind-curl line which is, presumably, due to the south–north excursion of the outcropping line shown in Fig. 5a. Adding these two layers together, there is a large-amplitude anticyclonic gyre in the subtropical basin, as shown in Fig. 5c. Finally, the thickness map of the fourth layer is shown in Fig. 5d. The abyssal water is dominated by a large cyclonic gyre.

To show the vertical stratification of the gyres, we present four vertical sections. Figure 6a shows a section at $y = 0.8$, approximately at the center of the subpolar gyre. The mixed layer is seen as a thin, constant depth ($H = 50$ m) layer on the top. The second layer cannot reach such a high latitude. The third layer appears as a small wedge of northward-flowing water on the upper-right corner. This feature is a crude simulation of the observed density structure in the subpolar gyre of the North Atlantic (cf. Worthington and Wright, 1972). Within the western basin at this latitude there is only one moving layer below the mixed layer, and the wind curl drives a cyclonic gyre in this layer. This cyclonic gyre is indicated by the upward displacement of the lowest interface. The sharp downward slope near the western wall implies a strong western boundary current flowing southward. The boundary current in the fourth layer mimics the deep western boundary current in the deep circulation theory by Stommel (1958). We will discuss this in more detail later.

A second section is at $y = 0.3$ (Fig. 6b) which is approximately through the center of the subtropical gyre. The configuration of the thermocline is typical
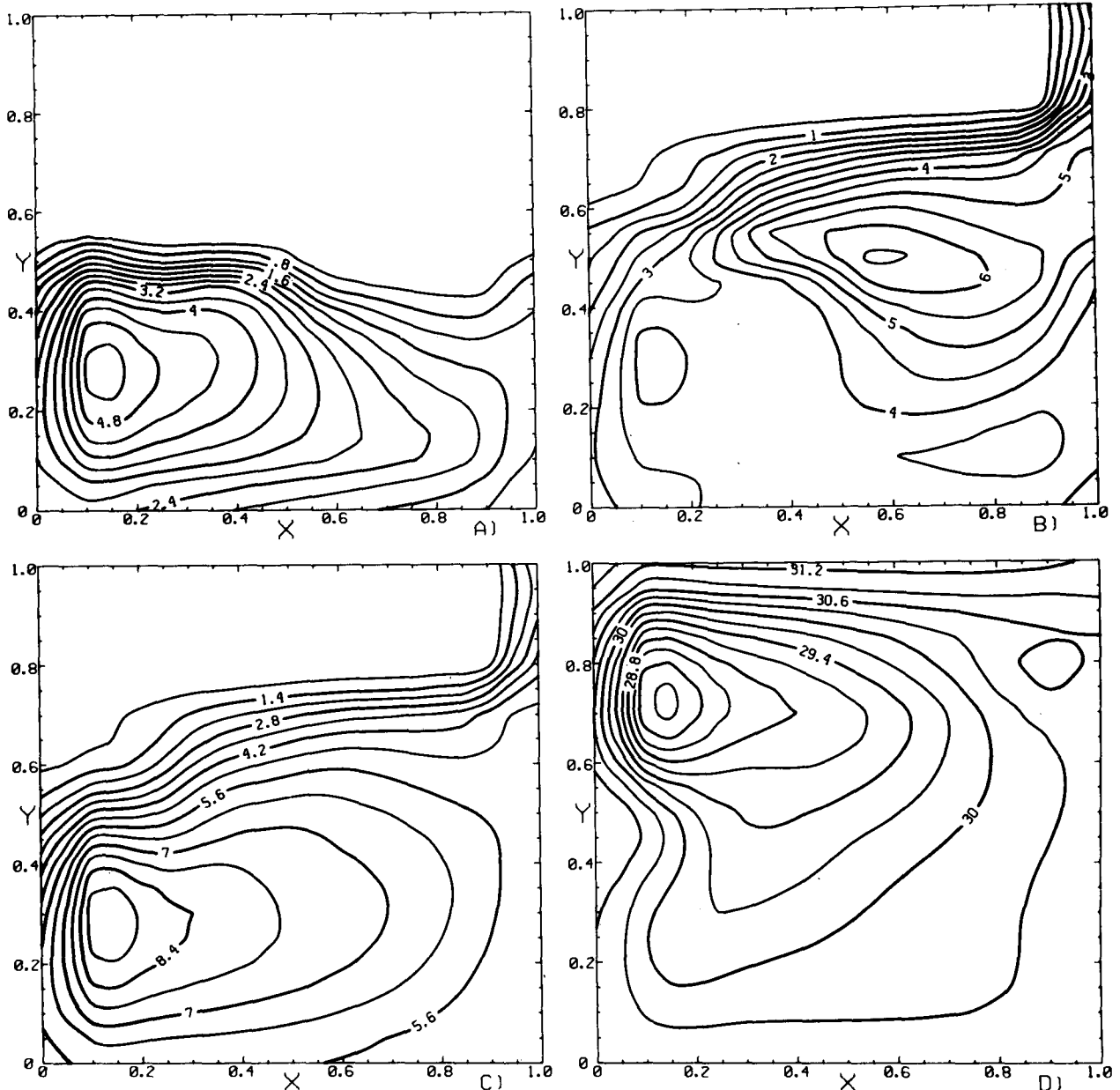
FIG. 5. Layer thickness and interface depth map, in units of hundred meters: (a) the second layer thickness; (b) the third layer thickness; (c) the depth map for the interface between the third and fourth layers; (d) the depth map of the lowest interface.

for a east–west hydrographic section in a subtropical basin. Except near the western boundary, the two upper interfaces gradually slope down westward, which implies a broad, slow southward motion in these two layers. The sharp upward tilt of these isopycnals near the western wall indicates a strong western boundary current. The distortion of the lowest interface suggests that there is a much weaker cyclonic circulation in the fourth layer, compared with the circulation fourth layer in the subpolar basin.

A third section at $x = 0.2$ clearly shows the subtropical gyre structure, Fig. 6c. Both the two upper

isopycnals indicate northern intensification of the subtropical gyre. The difference in the strength of the lowest interface distortion also shows that the motion in the fourth layer is much stronger in the subpolar basin than in the subtropical basin. This is so because the fourth layer is directly forced by wind stress (or Ekman pumping) in the subpolar basin, while in the subtropical basin the fourth layer is sheltered from direct forcing.

The fourth section is at $x = 0.8$, in the center of the eastern basin. One important difference between Figs. 6c and 6d is that starting from midlatitudes, the layer thickness increases southward in Fig. 6c, while it de-
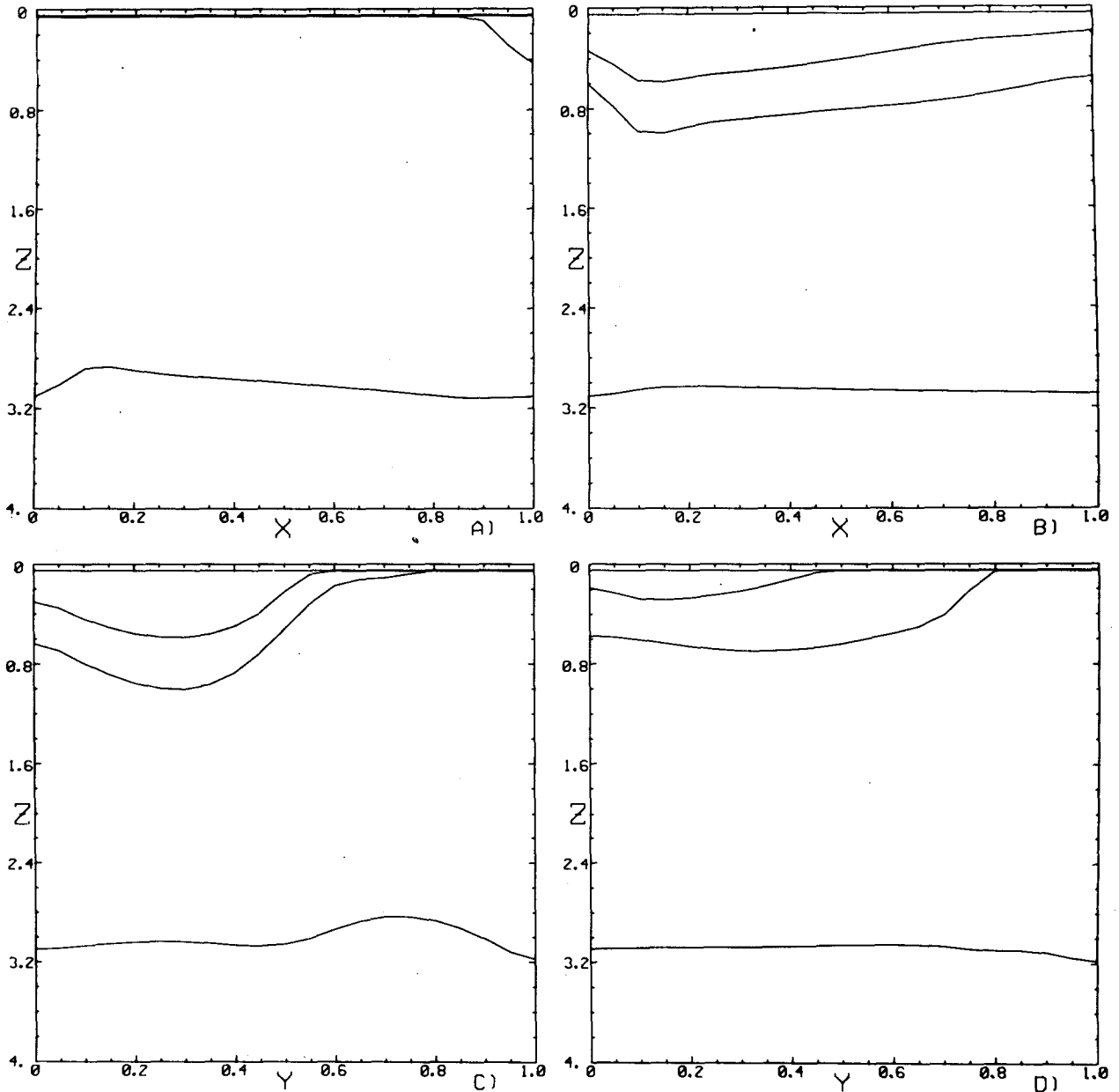
FIG. 6. Vertical sections of the basin: (a) $y = 0.8$, showing the northward warm water on the upper right corner; (b) $y = 0.3$, showing the subtropical gyre with its western boundary current on the left; (c) $x = 0.2$, showing the northern intensification of the subtropical gyre; (d) $x = 0.8$.

creases southward in Fig. 6d. As will be pointed out later, the western intensification of the subtropical gyre creates high potential vorticity by strong lateral momentum mixing and interfacial friction. This high potential vorticity water mass is transformed into low potential vorticity water by convective adjustment processes taking place in the western boundary outflow region. Therefore, the water column in the eastern basin is greatly destratified compared with the western basin. Our results here are similar to Cox and Bryan (1984) and Takeuchi (1984).

Our next step is to examine the velocity field. An arbitrary two-dimensional velocity field can always be represented in terms of a streamfunction and a streampotential. We have presented the streamfunction in Figs. 7, 8 and 11 and streampotential in Fig. 12. Before going into detail, the reader should be reminded that the real velocity patterns (vertically integrated through each layer) consist of divergent and nondivergent components. We put in arrows to indicate the overall flow pattern. However, the reader is to be reminded that streamfunction contours are not exactly streamlines,

especially within regions of strong convective adjustment, upwelling, and downwelling. Since we define the mass streamfunction to be zero at the lateral boundaries, dense packing of streamfunction contours do not necessarily mean a strong boundary current. Near both the southern and northern boundaries densely packed streamfunction contours are created by strongly divergent flow associated with upwelling and downwelling.

Let us begin with the mass streamfunction map of the mixed layer, Fig. 7a. There are apparently three gyres in the mixed layer, an anticyclonic gyre in the midlatitude and two cyclonic gyre-looking patterns near the southern/northern boundaries. Actually, near the southern/northern boundaries all these dense streamfunction contours do not represent streamlines: they are created by strong upwelling/downwelling along these boundaries, and thus should be ignored. Water mass flux is supplied by strong upwelling near the southern boundary, and lost to the subsurface layer by strong downwelling near the northern boundary. The total velocity is northwestward near both the southern and northern boundaries. Another interesting point is that the western boundary current in the mixed layer separates from the western wall at a rather high latitude, just slightly south to the zero-wind line $y = 0.75$. The mass flux in the mixed layer is about 6 Sv (Sv $\equiv 10^6$ m^3 s^{-1}), which is much less than the total mass flux of the interior flow.

The mass streamfunction map of the second layer shows a typical subtropical gyre carrying a mass flux of 24 Sv, which is a major part of the total mass flux of the barotropic transport.

The mass streamfunction map of the third layer is probably the most interesting one. As seen from Fig. 8, there is an anticyclonic gyre in the southern basin, while there is one-half of a cyclonic gyre in the northern basin. The mass flux in the anticyclonic gyre carries about 16 Sv and the cyclonic gyre carries 8 Sv of transport, most of which is actually derived by convection from the second layer. Eventually this poleward-moving water in the third layer sinks to the fourth layer after reaching high latitudes. This will become much clearer later when we discuss the source distribution in each layer.

The potential vorticity map of the third layer is very similar to the numerical result of the GFDL eddy-resolving primitive equation model (Cox, 1985). There is a low potential-vorticity tongue in the western basin, and high potential-vorticity tongue jutting out from the eastern boundary. There is also high vorticity in the western boundary current region.

In Fig. 9 we reproduce a potential vorticity map compiled by McDowell et al. (1982). This map shows the potential vorticity along an isopycnal surface in the interval sigma-theta equal to 26.3–26.5. The principal features in the North Atlantic are a tongue of high potential vorticity, well-stratified water along the equatorward flank of the subtropical gyre in the western sector. There is another region of high potential vorticity near the western boundary. In between is a broad region of lower potential vorticity water that appears to have undergone winter convection before being swept southward into the main thermocline. Corresponding features have been reported in the potential vorticity pattern for the North Pacific (Keffer, 1985).
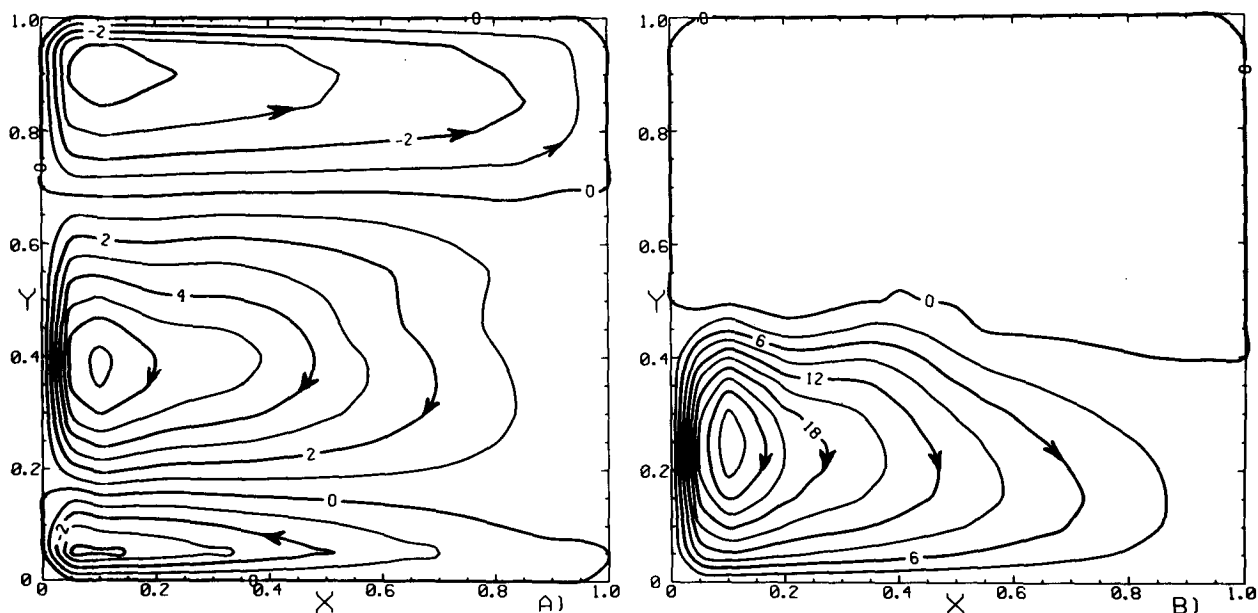

FIG. 7. Mass streamfunction maps of: (a) the mixed layer, (b) the second layer, in units of 10^6 m^3 s^{-1} (Sv).
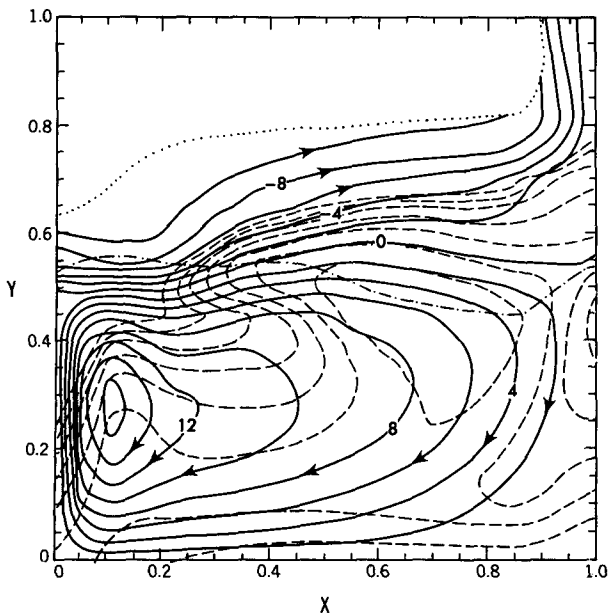
FIG. 8. Mass streamfunction [solid lines, in units of 10^6 m^3 s^{-1} (Sv)] and potential vorticity (dashed lines, increasing northward along the eastern boundary with intervals of 2×10^{-10} cm^{-1} s^{-1}) of the third layer. To keep the picture clear, contours near the separation latitude and the second outcropping line with values higher than 3.1 $\times 10^{-9}$ are not shown. The dotted line is the outcropping line of the third layer, and the dot–dash line is the outcropping line of the second layer.

FIG. 9. Potential vorticity at $\sigma_\theta = 26.3–26.5$ in the North Atlantic (adapted from McDowell et al., 1982).

The flow pattern and distribution of potential vorticity are shown for the third layer of the model in Fig. 10. The dotted line indicates the outcrop line of this layer, while the dash–dot line indicates the outcrop of the overlying layer. Between the dotted line and dash–dot line the third layer is in direct contact with the surface mixed layer. Equatorward of the dash–dot line the layer is not directly forced. LPS refer to the flow of one layer under another layer as subduction. Note that active subduction is taking place near the eastern boundary, bringing relatively high potential vorticity waters into the subtropical gyre region. This feature is very much like the tongue shown in McDowell's pattern in the previous figure. In this center of the gyre there is also a region of low potential vorticity in the model corresponding to observations. As we trace back along the streamlines it can be seen that the low potential vorticity emanates from a stippled region. The light stipples indicate convection and the heavy stipples very intense convection.

Within the context of our simple layered model, convection reduces the thickness of the layer in contact with the mixed layer and increases the thickness of the next layer below as shown in Fig. 2. This implies that thickness is increased in convective areas equatorward of the dash–dot line. There is a marked gradient in potential vorticity along trajectories in the convective region, but no gradient in potential vorticity along tra-
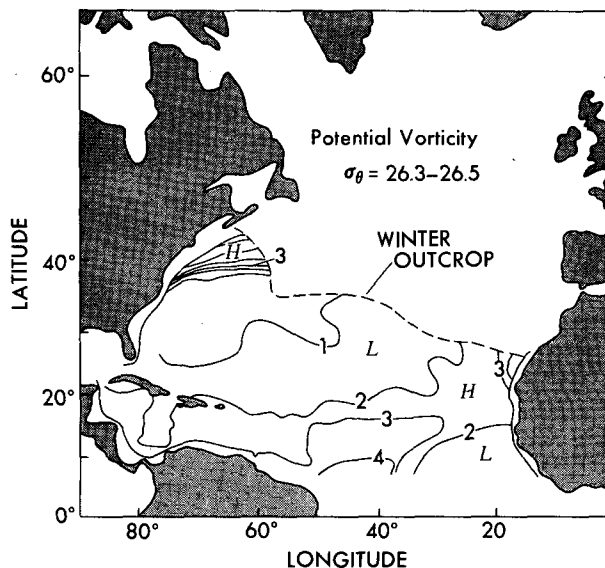
jectories poleward of the outcrop line where convection is suppressed. This creates a pronounced kink in the potential vorticity pattern along the outcrop line.

In the western boundary current region there is a sharp gain of potential vorticity along the trajectories. This is probably due to strong interface friction and lateral friction implemented in the model. The poten-
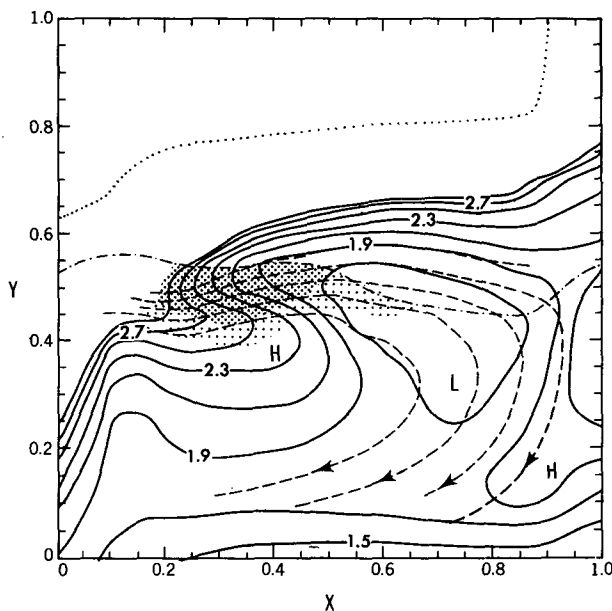

FIG. 10. Potential vorticity (solid lines) and streamfunction (dashed lines) of the third layer. Light stippled area for the source region with intensity less than 2×10^{-4} cm s^{-1}, and heavy stippled area for the region with source intensity larger than 2×10^{-4} cm s^{-1}.

tial vorticity balance, however, required detailed analysis of the model, which will be reported later.

The overall regime is very similar to that described by Cox and Bryan (1984). As we trace along streamlines which have closed trajectories and which pass through the stippled region, it can be seen that in the interior potential vorticity is approximately conserved. A great increase of potential vorticity takes place in the western boundary current region. This is largely balanced by convection at the upper boundary of the gyre which reduces the potential vorticity back to its interior value.

The mass streamfunction in the fourth layer shows a single cyclonic gyre with a total mass flux of 16 Sv, as shown in Fig. 11. The other part of the velocity field comes from the source distribution within each layer. Physically, the source map is a map of the difference in the diapycnal velocity entering a layer and that leaving the layer, plus the contribution from convective adjustment. As seen from Fig. 12a, there is a broad sink (Ekman pumping) region in the subtropical basin and a broad source (Ekman suction) region in the subpolar basin. At the western boundary there is a strong upwelling south to the zero-wind-curl line. Along the southern (northern) boundary there is a strong upwelling (downwelling) which is required by mass compensation of the mixed layer flow driven by local easterly winds.

The source map of the second layer shows quite different regions. A broad source region in the interior subtropical basin is apparently an algebraic sum of the Ekman pumping of the mixed layer and the diapycnal

mixing between the second and third layers. The strong source and sink near the western boundary are probably connected with the upwelling and downwelling. Of greatest interest is the source region in the center of the basin. Obviously, this is the place where convective adjustment takes place and warm water in the second layer sinks down to the third layer. This can be confirmed by the source map of the third layer where one finds a strong source area just below the corresponding sink region of the second layer. These two areas apparently have equal strengths. This convective adjustment and the associated low potential vorticity water mass formation are very similar to the results found in Cox and Bryan (1984) and the real process taking place in the Sargasso Sea. By examining the source/sink map of the third layer, one finds a strong sink area in the northeast corner which corresponds to a deep water formation region, probably the Norwegian Sea in the North Atlantic. The broad interior of the third layer has a small source distribution which is due to the slow upwelling from the abyss.

There is a strong source in the fourth layer near the poleward wall. There is also a broad weak sink in the interior which corresponds to slow upwelling of abyssal waters.

By combining Figs. 8, 11 and 12, one finds a very simple picture similar to the scheme proposed by Stommel (1958) for the deep circulation. In a thermally driven basin, warm surface water is cooled down at places such as the Northwest Atlantic and the Norwegian Sea. That is also the place where Budyko's map indicates a major heat loss to the atmosphere.

The deep water formed in the northeast corner by convective adjustment flows westward along the northern boundary, turns southward when it meets the western boundary, and becomes a deep western boundary current. Water in this deep boundary current gradually returns to the interior and moves upward through the thermocline. This slow upward motion provides a source for the interior ocean which drives a broad northward flow.

4. Conclusions

The main contribution of this study is the demonstration of a new tool for understanding the ocean circulation. The isopycnal coordinate system and the representation of the thermocline and abyssal waters as three moving layers below a mixed layer allows an extremely simple, but nontrivial model of the thermohaline and wind-driven circulation. The model is semi-Lagrangian in the sense that ideal adiabatic flow would be exactly parallel to the isopycnal coordinates. One of the great advantages of this coordinate representation, as pointed out by Hoskins et al. (1985), is that we can apply potential vorticity ideas directly to the solutions without the complicated diagnostic procedures.
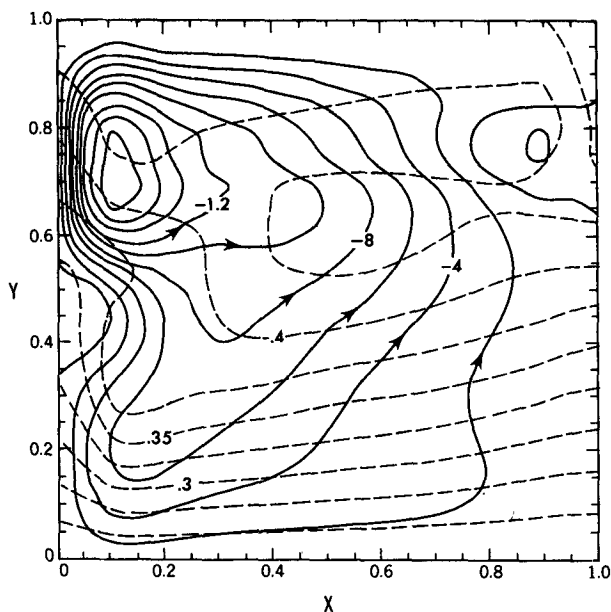

FIG. 11. Mass streamfunction [solid line, in units of 10^6 m^3 s^{-1} (Sv)] and potential vorticity (dashed lines, in units of 10^{-9} cm^{-1} s^{-1}) of the fourth layer.
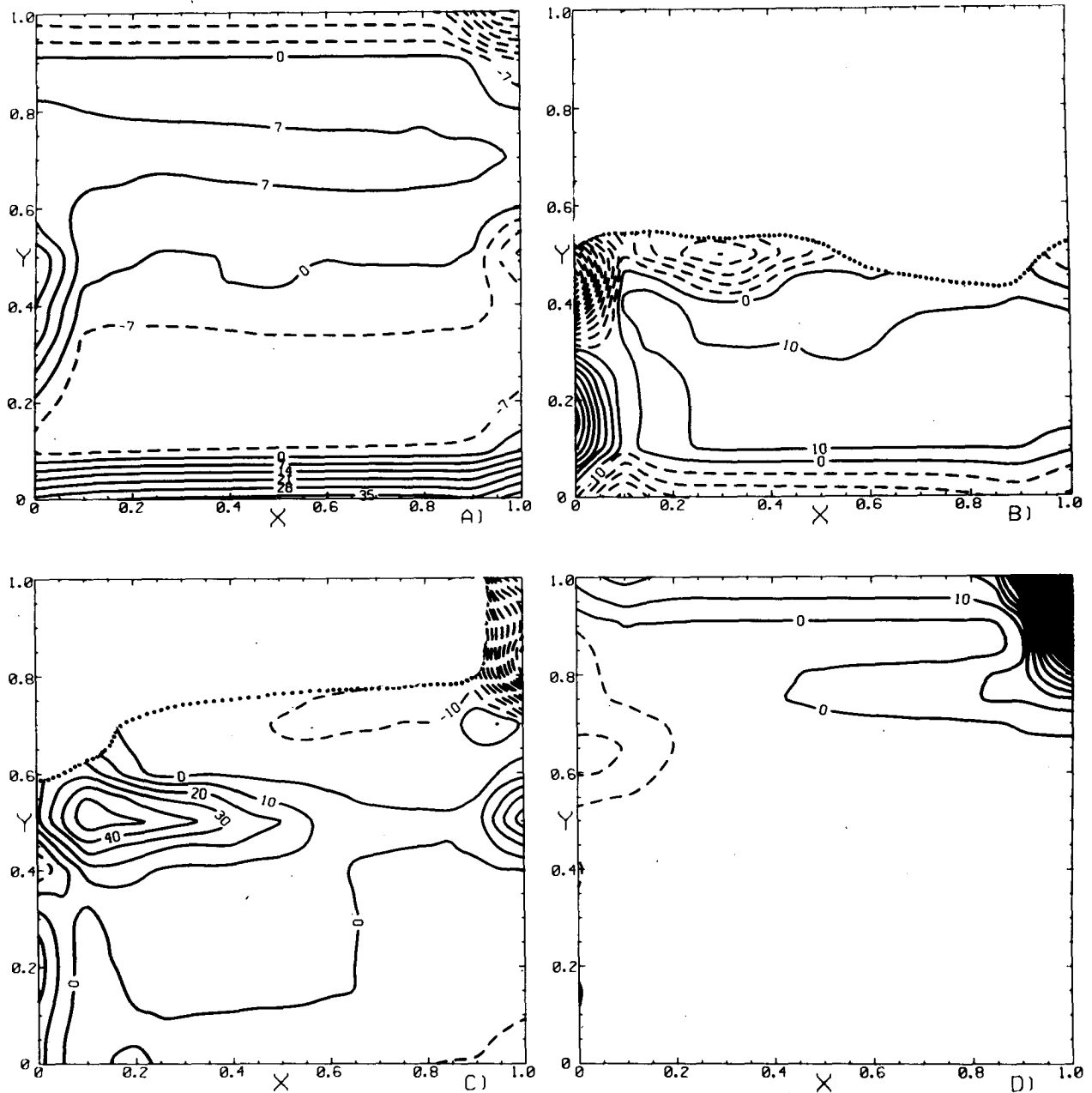
FIG. 12. Source distribution (in units of 10^{-5} cm^1 s^{-1}), dashed contours for sink. (a) the mixed layer; (b) the second layer; (c) the third layer; and (d) the fourth layer. Dotted lines are the outcropping lines.

We conclude that our method is adequate to reproduce important features of the potential vorticity field in the main thermocline found in observations, although our model has much less resolution than previous models based on fixed Eulerian coordinates. In addition, the present model with a small number of moving layers offers far more physical insight than Eulerian models. Essentially, the isopycnal coordinates reduce the three-dimensional solution to a small number of two-dimensional flows which are linked together

by areas of strong upwelling, sinking, or slow diapycnal mixing.

The interaction of convection with large-scale flow in the ocean is usually considered to be extremely difficult to include in any analytic model. For this reason, little progress has been made in understanding its role in the ocean circulation. An important part of our model is a very simple representation of convection which allows it to be seen in its simplest terms. In the context of our simple layered model, convection is a

constraint which does not allow the mixed-layer density to exceed that of the underlying layer. To conserve buoyancy in the water column, the change of buoyancy in the mixed layer must be balanced by a redistribution of thickness in the layers below. In most cases the layer in contact with the mixed layer is thinned. In extreme cases it will disappear altogether. The model shows in a very simple way the dominant impact of convection in the subarctic gyre as well as its less important, but still very significant role in the subtropical gyre through its effect on the potential vorticity of ventilated water.

The present model is only adequate to represent very large-scale features of the ocean circulation. Only by extending model calculations to the eddy-resolving scale can a model determine its own diffusivity. Bleck and Boudra (1981, 1986) have made initial tests of an eddy-resolving model based on isopycnal coordinates, but much work remains to be done to ensure that such a model accurately simulates baroclinic and barotropic instability of mesoscale eddies. To discuss the role of the ocean in the global heat balance, heat and salinity must be included as separate components in the model with a realistic equation of state. The complexity of the equation of state for sea water is a rich source of nonlinearity and leads to possible multiequilibrium solutions. This complexity has yet to be explored in global numerical models.

In analytical theories of the thermocline, different idealizations have to be applied to make the problems analytically solvable. For example, in the LPS model thermocline flow is assumed to be "ideal" in the sense that potential vorticity and density are conserved along geostrophic trajectories. In the generalized Parsons' model (e.g., Huang and Flierl, 1987), neither diapycnal nor isopycnal mixing is allowed, thus each layer has a constant volume of water. A numerical model will not ordinarily be able to simulate such flows. However, this may not be such a serious drawback in the light of recent evidence from drifters (e.g., see Krauss and Boening, 1986) that flow in the thermocline is far from "ideal" and diffusion of potential vorticity along isopycnal surfaces by mesoscale eddies is a first-order process in the North Atlantic.

In terms of upper boundary conditions on density, the LPS model and the generalized Parsons' model represent two extremes in the specification of boundary conditions at the upper surface. In the LPS model a density distribution is imposed which is physically equivalent to an overlaying atmosphere of infinite heat capacity. In the generalized Parsons' model surface density is determined through global dynamical balance. It is only with a numerical model that one can study the continuous range between these two extremes. In fact, our numerical experiments have shown some interesting cases in this connection, and the results will be presented in future studies which will also be supplemented by a more dynamical description in terms of potential vorticity balance.

APPENDIX

The Turbulent Density Flux Across the Bottom of the Mixed Layer

For numerical models, it is important to have some basic quantities conserved exactly. As for our simple model, we have chosen to conserve both the total volume and buoyancy. Although the volume conservation is rather easy to maintain, the buoyancy conservation is not as easy as it seems to be at first glimpse. For the constant density layers, the buoyancy conservation principal emerges as a means of determining the diapycnal velocity, Eq. (12). Thus, the remaining issue is to define the interface buoyancy flux on the boundary between these two coordinate systems.

A possible numerical scheme is to use an upwind scheme to define the buoyancy flux between layers and use the buoyancy conservation law to predict the time evolution of the density for individual layers. Although this approach conserves both total volume and buoyancy, and leads to a convergent solution, the grid spacing in the density coordinate evolves with time. This coordinate drift can lead to closely packed coordinate surfaces, a rather undesirable feature.

As an alternative approach we have chosen to constrain the density in each layer to have a constant value. To assure that both mass and buoyancy are conserved globally in the hybrid coordinate system requires a very specific definition of the buoyancy flux between the mixed layer and the moving layer below. To derive the buoyancy flux required, let us start with a general form of the density conservation law

$$\partial \rho / \partial t + \nabla(\rho \mathbf{u}) = -\nabla \mathbf{F} \qquad (A1)$$

where ∇ is a three-dimensional divergence operator and $\mathbf{F}$ is the turbulent density flux. Since isopycnal coordinate is used, $\mathbf{F}$ has only diapycnal components. Integrating (A1) over a vertical water column below the mixed layer with unit horizontal section gives

$$\frac{\partial}{\partial t} \iiint \rho \, dv + \iint \rho u_n \, ds = -\iint F_n \, ds, \qquad (A2)$$

where u_n and F_n are the velocity and turbulent flux normal to the surface of the volume. If we write the left-hand side of (A2) in discrete form we have

$$\sum_{k=2}^{4} [\partial/\partial t h_k \rho_k + \rho_k \nabla_\rho (h_k \mathbf{u}_k^h)] + w_e \rho_2 = -F_s, \qquad (A3)$$

where $\mathbf{u}_k^h$ is the horizontal velocity of the kth layer, ∇_ρ is a two-dimensional operator defined on the isopycnal surface, w_e is the vertical velocity across the upper interface, and F_s is the corresponding turbulent density flux at the upper interface. Note that the buoyancy conservation for constant density layer requires an upper boundary buoyancy flux defined as $w_e \rho_2$, and a no buoyancy flux condition has been used for the lowest boundary.

Substituting (13) into (A3) gives the turbulent buoyancy flux at the upper interface

$$F_s = w_{23}^*(\rho_3 - \rho_2) + w_{34}^*(\rho_4 - \rho_3) \qquad \text{(A4)}$$

where w_{23}^* and w_{34}^* are the diapycnal velocity across the interface between the second and third layer and between the third and fourth layer. Substituting (29, 30) into (A4), one obtains

$$F_s = \frac{1}{2}\mu[(\Delta\rho_2 + 2\Delta\rho_1)/h_2 - (\Delta\rho_3 + \Delta\rho_4)/h_4]. \qquad \text{(A5)}$$

Equations (A3, 4, 5) are valid only if the second layer has nonzero thickness. When the lower layers outcrop, this relation should be modified to an appropriate form.

REFERENCES

Bleck, R., and D. B. Boudra, 1981: Initial testing of a numerical ocean circulation model using a hybrid (quasi-isopycnic) vertical coordinate. *J. Phys. Oceanogr.*, **11**, 755–770.
——, and ——, 1986: Wind-driven spin-up in eddy-resolving ocean ocean models formulated in isopycnic and isobaric coordinates. *J. Geophys. Res.*, **91**, 7611–7621.
Bougue, N. M., R. X. Huang and K. Bryan, 1986: Verification experiments with an isopycnal coordinate ocean model. *J. Phys. Oceanogr.*, **16**, 985–990.
Boris, J. P., and D. L. Book, 1973: Flux-corrected transport. I. SHASTA, A fluid transport algorithm that works. *J. Comput. Phys.*, **11**, 38–69.
Bryan, K., 1969: A numerical method for the study of the circulation of the world ocean. *J. Comput. Phys.*, **4**, 347–376.
——, 1984: Accelerating the convergence to equilibrium of ocean-climate models. *J. Phys. Oceanogr.*, **114**, 666–673.
——, and L. J. Lewis, 1979: A water mass model of the world ocean. *J. Geophys. Res.*, **84**, 2503–2517.
Budyko, M. I., 1963: *Atlas of the Heat Balance of the Earth Sphere.* Joint Geophysical Committee, Presidium of the Academy of Sciences, Moscow, 5 pp., 69 plates.
Cox, M. D., 1985: An eddy resolving numerical model of the ventilated thermocline. *J. Phys. Oceanogr.*, **15**, 1312–1324.
——, and K. Bryan, 1984: A numerical model of the ventilated thermocline. *J. Phys. Oceanogr.*, **14**, 674–687.
Hodnett, P. F., 1978: On the advective model of the thermocline circulation. *J. Mar. Res.*, **35**, 185–198.
Holland, W. R., T. Keffer and P. B. Rhines, 1984: Dynamics of the oceanic general circulation: The potential vorticity field. *Nature*, **308**, 698–705.
Hoskins, B. J., M. E. McIntrye and A. W. Robertson, 1985: On the use and significance of isotropic potential vorticity maps. *Quart. J. Roy. Meteor. Soc.*, **111**, 877–946.
Huang, R. X., 1984: The thermocline and current structure in subtropical/subpolar basins. Ph.D. thesis, Massachusetts Institute of Technology, Woods Hole Oceanogr. Inst. Tech. Rep., **84-42**, 218 pp.
——, 1986: Numerical simulation of wind-driven circulation in a subtropical/subpolar basin. *J. Phys. Oceanogr.*, **16**, 1636–1650.
——, 1987: A three-layer model for wind-driven circulation in a subtropical-subpolar basin. Part I. Model formulation and the

subcritical state. Part II. The supercritical and hypercritical states. *J. Phys. Oceanogr.*, **17**, 664–678; 679–697.
——, and G. Flierl, 1987: Two-layer models for the thermocline and current structure in subtropical/subpolar gyres. *J. Phys. Oceanogr.*, **17**, 872–884.
Kamenkovich, V. M., and G. M. Reznik, 1972: A contribution to the theory of stationary wind-driven currents in a two-layer liquid. *Izv. Akad Sci. USSR, Atmos. Oceanic Phys.*, (Engl. Transl.), **8**, 238–245.
Keffer, T., 1985: The ventilation of the world's oceans: Maps of the potential vorticity field. *J. Phys. Oceanogr.*, **15**, 509–523.
Killworth, P. D., 1985: A two-level wind and buoyancy driven thermocline model. *J. Phys. Oceanogr.*, **15**, 1414–1432.
Krauss, W., and C. W. Boening, 1986: Lagrangian properties of eddy fields in the northern North Atlantic as deduced from satellite-tracked buoys. *J. Mar. Res.*, submitted.
Luyten, J. R., and H. Stommel, 1986: Gyres driven by combined wind and buoyancy flux. *J. Phys. Oceanogr.*, **16**, 1551–1560.
——, J. Pedlosky and H. Stommel, 1983: The ventilated thermocline. *J. Phys. Oceanogr.*, **13**, 292–309.
McDougall, T. J., and J. A. Church, 1986: Pitfalls with the numerical representation of isopycnal and diapycnal mixing. *J. Phys. Oceanogr.*, **16**, 196–199.
McDowell, S., P. B. Rhines and T. Keffer, 1982: North Atlantic potential vorticity and its relation to the general circulation. *J. Phys. Oceanogr.*, **12**, 1417–1436.
Mesinger, F., and A. Arakawa, 1976: Numerical methods used in atmospheric models. GARP Publication Series No. 14, WMO/ICSU Joint Organizing Committee, 64 pp.
Moum, J. N., and T. R. Osborn, 1986: Mixing in the main thermocline. *J. Phys. Oceanogr.*, **16**, 1250–1259.
Parson, A. T., 1969: A two-layer model of Gulf Stream separation. *J. Fluid Mech.*, **39**, 511–528.
Pedlosky, J., 1986: The buoyancy and wind-driven ventilated thermocline. *J. Phys. Oceanogr.*, **16**, 1077–1087.
——, W. Smith and J. R. Luyten, 1984: On the dynamics of the coupled mixed layer-thermocline system and the determination of the oceanic surface density. *J. Phys. Oceanogr.*, **14**, 1159–1171.
Redi, M. H., 1982: Oceanic isopycnal mixing by coordinate rotation. *J. Phys. Oceanogr.*, **12**, 1154–1158.
Rhines, P. B., and W. R. Young, 1982: A theory of the wind-driven circulation, Part I. *J. Mar. Res.*, **40**(Suppl.), 559–596.
——, W. R. Holland and J. Chow, 1985: Experiments with buoyancy-driven ocean circulation. NCAR Tech. Note, NCAR/TN-260+str, 108 pp.
Robinson, A. R., 1965: A three-dimensional model of inertial currents in a variable-density ocean. *J. Fluid Mech.*, **21**, 211–223.
Stommel, H., 1958: The abyssal circulation. *Deep-Sea Res.*, **5**, 80–82.
Takeuchi, K., 1984: Numerical study of the subtropical front and the subtropical countercurrent. *J. Oceanogr. Soc. Japan*, **40**, 371–381.
Veronis, G., 1973: Model of world ocean circulation: I. wind-driven two-layer. *J. Mar. Res.*, **31**, 228–288.
Welander, P., 1966: A two-layer frictional model of wind-driven motion in a rectangular oceani basin. *Tellus*, **18**, 54–62.
Worthington, L. V., and W. R. Wright, 1972: *North Atlantic Ocean Atlas of Potential Temperature and Salinity, and Oxygen Profiles from the Erika Dan Cruise of 1962.* Woods Hole Oceanographic Institution Atlas Series 2, 24 pp.
Zalesak, S. T., 1979: Fully multidimensional flux-corrected transport algorithms for fluids. *J. Comput. Phys.*, **31**, 335–362.